

Enhanced tensile strength and ductility of bulk metallic glasses $\text{Zr}_{52.5}\text{Cu}_{17.9}\text{Al}_{10}\text{Ni}_{14.6}\text{Ti}_5$ via high-pressure torsion

Zhi Qiang Ren^a, A.A. Churakova^{b,c}, Xiang Wang^a, Sunkulp Goel^a, Si Nan Liu^a, Ze Sheng You^a, Ying Liu^a, Si Lan^a, D.V. Gunderov^{b,c}, Jing Tao Wang^{a,*}, R.Z. Valiev^{c,d}

^a School of Materials Science and Engineering, Nanjing University of Science & Technology, Nanjing, 210014, China

^b Institute of Molecule and Crystal Physics, Ufa Federal Research Center RAS, Ufa, 450075, Russia

^c Ufa State Aviation Technical University, 12 K. Marx Str, Ufa, 450008, Russia

^d Saint Petersburg State University, 28 Universitetskiy Pr., Saint Petersburg, 198504, Russia



ARTICLE INFO

Keywords:

Amorphous-crystalline composites
Tensile ductility
Strength
Free volume
Inter-crystallite spacing
Ductilization window

ABSTRACT

$\text{Zr}_{52.5}\text{Cu}_{17.9}\text{Al}_{10}\text{Ni}_{14.6}\text{Ti}_5$ (Vit105) Bulk metallic glass is processed by High-Pressure Torsion up to 30 rotations at room temperature, showing simultaneous enhancement of both strength (2023 MPa) and ductility (0.45%). Nano-crystal precipitates with an average size of 45 nm inside the amorphous matrix are observed after 30 turns HPT. Free volume increases from $\sim 0.9030 \text{ \AA}^3$ (as cast) to $\sim 0.9275 \text{ \AA}^3$ after 30 turn HPT alloy with 2.83% (by volume) of nanocrystal precipitates. Strengthening due to precipitation after 30 turns HPT comply with the phase mixture model. The synergistic effect of free volume and nanocrystal precipitation on the ductility of amorphous-crystallite composite is quantitatively approached through modelling. By implementing the model, a ductilization window between bottom limit and top limit of the inter-crystallite spacing w.r.t the free volume is established, elucidating the necessary conditions required to obtain plasticity in amorphous-crystalline composites.

1. Introduction

Bulk Metallic Glasses (BMGs) have been extensively studied for their excellent mechanical properties, such as mechanical strength and hardness [1,2]. However, it has been frequently observed that some BMGs are brittle at room temperature [3–6], and various strategies have been developed to improve the mechanical properties of BMGs, especially ductility [7–10]. Among these efforts, surface heterogeneous structure introduced by surface treatment of amorphous alloys [11,12], and compositing with crystalline inclusions in the amorphous matrix come out to be effective approaches to improve the tensile plasticity [13–16]. The amorphous-crystalline composites can be prepared by solidification through the pre-crystallization of soft ductile dendrite phase, which leads to significant improvements of the composite ductility with some decrease in strength compared to their monolithic BMGs counterpart [13,14]. Thermal annealing can also introduce crystallites in the BMGs matrix [15,16]. After annealing, the strength of BMGs may increase due to the strengthening effect of precipitated nanocrystals [17–19]. However, annealing might cause brittleness or reduction of plasticity in BMGs [20,21], since annealing could lead to

the reduction of the free volume which subsequently decrease its intrinsic ductility [22], although enhancement of ductility might be possible through deflecting the active shear bands assisted by the precipitated nanocrystals [23,24]. Severe plastic deformation processing emerges to be a favorable approach for improving the microstructure and properties of crystalline materials, and it seems to be true also for the BMGs. It has been proved that plastic deformation produced multiple shear bands in BMGs and increases free volume in the alloy, thereby enhancing the ductility, sometimes at the expense of yield strength [25,26]. The above examples indicate that difference in processing route to achieve amorphous-crystalline composites consequent upon different behavior of ductility and strength of the composites. A systematic understanding of the enhancing mechanism on strength and ductility will be of great benefits for further enlightenment on development and processing of high property BMGs comprehensively. Moreover, it would be interesting to explore the possibility of improving both strength and ductility at the same time, by applying the amorphous-crystalline composites strategy.

Since, severe plastic deformation generates additional free volume imparting ductility and formation of nanocrystal precipitates

* Corresponding author.

E-mail address: jtwang@njust.edu.cn (J.T. Wang).

incorporate strengthening, it is thus considered a potential method to improve both strength and ductility. In this paper, high-pressure torsion (HPT) with controlled processing parameter has been performed on Vit105 BMGs alloy with standard composition. The Synchrotron X-ray diffraction and transmission electron microscopy (TEM) are used to observe the microstructure change; tensile tests are used to characterize the strength and ductility, and modeling approaches to understand the comprehensive effect of enhanced strength and ductility, due to the formation of the additional free volume and nanocrystal precipitation after processing Vit105 BMGs by HPT.

2. Experimental

The Vit105 alloy ingots with a standard composition of $Zr_{52.5}Cu_{17.9}Al_{10}Ni_{14.6}Ti_5$ were prepared by arc melting using pure element metals of Zr, Cu, Ni, Al and Ti (purities better than 99.9%) under an argon atmosphere. The ingots were remelted four times for chemical homogeneity. The melt was subsequently cast into a water-cooled suction casting machine with a copper mold with a cylindrical cavity of 10 mm diameter. The Vit105 disc sample of 10 mm in diameter and 1 mm in thickness was placed on the 10 mm-diameter HPT anvils with a 0.3 mm-deep groove. In the process of HPT, the discs were deformed at a rotation rate of 1 rpm under applied pressure of 6 GPa at room temperature (RT) while varying the number of revolutions [27, 28]. The microstructural features of the specimens were observed using high-resolution electron microscopy (HRTEM) with energy dispersive spectroscopy (EDS).

The pair distribution function (PDF) was analyzed using Synchrotron X-ray diffraction conducted at beamline 11-ID-C at the Advanced Photon Source, Argonne National Laboratory. The data was acquired by high-energy X-ray with beam size of $500 \times 500 \mu\text{m}$ and wavelength of 0.1173 \AA . Two dimensional diffraction patterns were obtained by a PerkinElmer amorphous silicon detector. The time for data acquisition for each pattern and data readout and saving was 1s and 4s, respectively. The static structure factor, $S(Q)$, can be obtained by processing the scattering data. From the Fourier transform of $S(Q)$, the reduced pair distribution function (PDF), $G(r)$, can be obtained, that is, $G(r) = (2/\pi) \times \int_0^{Q_{\max}} Q(S(Q) - 1)\sin(Qr)dQ$. Where, r is the real space distance and $Q = 4\pi\sin\theta/\lambda$. Here, θ is half of the scattering angle between the incident and scattered beam. λ is the X-ray wavelength.

The mechanical properties of the specimens were evaluated using tensile tests. A miniature sized tensile specimen shown in Fig. 1 was used, to reduce the scatter of tensile data from the possibly occasional

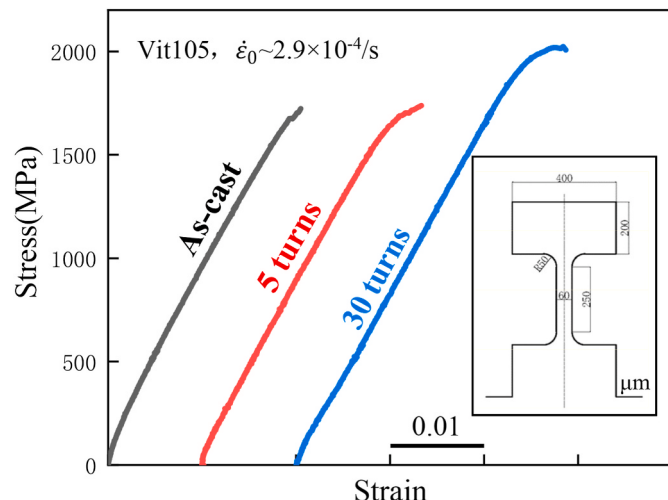


Fig. 1. Stress-strain curves of the as-cast and HPT-processed Vit105 BMGs. The inset shows the dimension of the tensile specimen.

un-recognizable flaws and other defects in the materials. Tensile displacement rate used for the test is $\sim 0.1 \mu\text{m/s}$, corresponds to an initial strain rate $\dot{\epsilon}_0$ of $\sim 2.9 \times 10^{-4}/\text{s}$. The strain in the gauge was accurately measured by a digital image correlation based non-contact gage. The high accuracy of the gage enables determinations of elastic modulus and plastic strain after yielding [29].

3. Results

Fig. 1 shows the tensile stress-strain curves of the as-cast sample, and samples after 5 turns or 30 turns of HPT processing. The as-cast alloy displays an elastic modulus E of $\sim 82 \text{ GPa}$ with no obvious tensile ductility, which is same as reported in literature with millimeter-sized or larger tensile samples [30,31]. This indicates that at the tensile sample scale used in the present work, size effect is still not enough to influence the mechanical behavior significantly.

Typical tensile stress-strain curves of the as-cast and HPT-processed Vit105 BMGs can be seen in Fig. 1. The different values obtained from the tensile stress strain curve, showing improvement in elongation and strength, after HPT are shown in Table 1. Yield point is defined as the point at which a stress plateau appears, or the point at around the first pop-in on the curve in case not obvious stress plateau [32]. In Vit105 BMGs, the yield strength is very close to the elastic limit [30,32,33]. The yield strength decreases from 1654 MPa of the as-cast sample to 1544 MPa after 5 turns HPT and thereafter increases again to 1793 MPa after 30 turns HPT. Meanwhile, the tensile strength and the plastic elongation increases from 1723 MPa and 0.06% of the as-cast sample to 2023 MPa and 0.45% after 30 turns HPT, respectively. Substantial enhancement of both strength and ductility is clearly observed after 30 turns of HPT. Fig. 2 shows the fracture morphology of the as-cast and 30 turns HPT specimen after tensile test. Shear veins can be observed on the fracture surface of all the samples, which is the typical tension shear fracture morphology of amorphous alloy [34,35]. The 30 turns HPT specimen shows more irregular shear veins, which usually relates to better tension ductility [35–37].

Fig. 3(a) shows the structure factors $S(Q)$ of the as-cast and HPT-processed BMGs. All the samples show a strong first peak accompanied by dramatically declined oscillations on the right side of the peak. Based on the peak position Q_1 of the first sharp diffraction peak, the atomic volume (V_a) was calculated by the formula $Q_1 \cdot V_a^{0.433} = 9.36$ [38]. Therefore, the atomic volume of the as-cast, 5 turns and 30 turns HPT specimen is 18.06 \AA^3 , 18.31 \AA^3 , 18.55 \AA^3 , respectively. The relationship between free volume (V_f) and atomic volume can be expressed as $V_f = V_a - V_0$ [39], where V_0 is the average atomic volume in the ideal glassy state, and V_a the average atomic volume obtained in this experiment. Assuming $V_a/V_0=n$, the atomic volume can be expressed as $V_a = V_f/(1-n)$ in terms of free volume. The free volume of as-cast specimen is reported to be 4.5%~6.7% of average atomic volume in the literature [40–42], obtained by DSC and XRD measurements. Taken 5% as a typical percentage of free volume to average atomic volume, which means the value of n is 0.95, the free volume of the as-cast, 5 turns and 30 turns HPT specimen could be estimated to be 0.9030 \AA^3 , 0.9155 \AA^3 , 0.9275 \AA^3 , respectively. A substantial increase of free volume in the HPT-processed BMGs was observed, in comparison to the as-cast specimen.

To better understand the atomic structure with such a significant free volume increase, the corresponding reduced pair distribution functions (PDF) [$G(r)$] is analyzed, as shown in Fig. 3(b). The PDFs show short to

Table 1
Mechanical properties of the as-cast and HPT specimen.

	YS (MPa)	UTS (MPa)	E (GPa)	Elongation(%)
As-cast	1654	1723	83.4	0.06
5 turns	1544	1738	81.5	0.29
30 turns	1793	2023	82.4	0.45

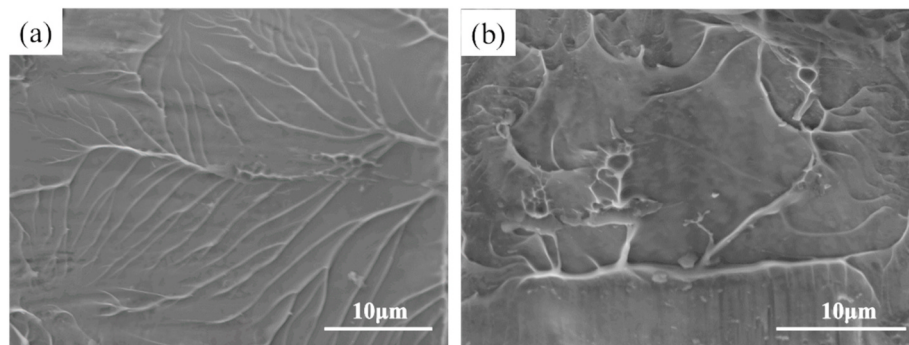


Fig. 2. The fracture morphology of (a) as-cast and (b) 30 turns HPT tensile specimen.

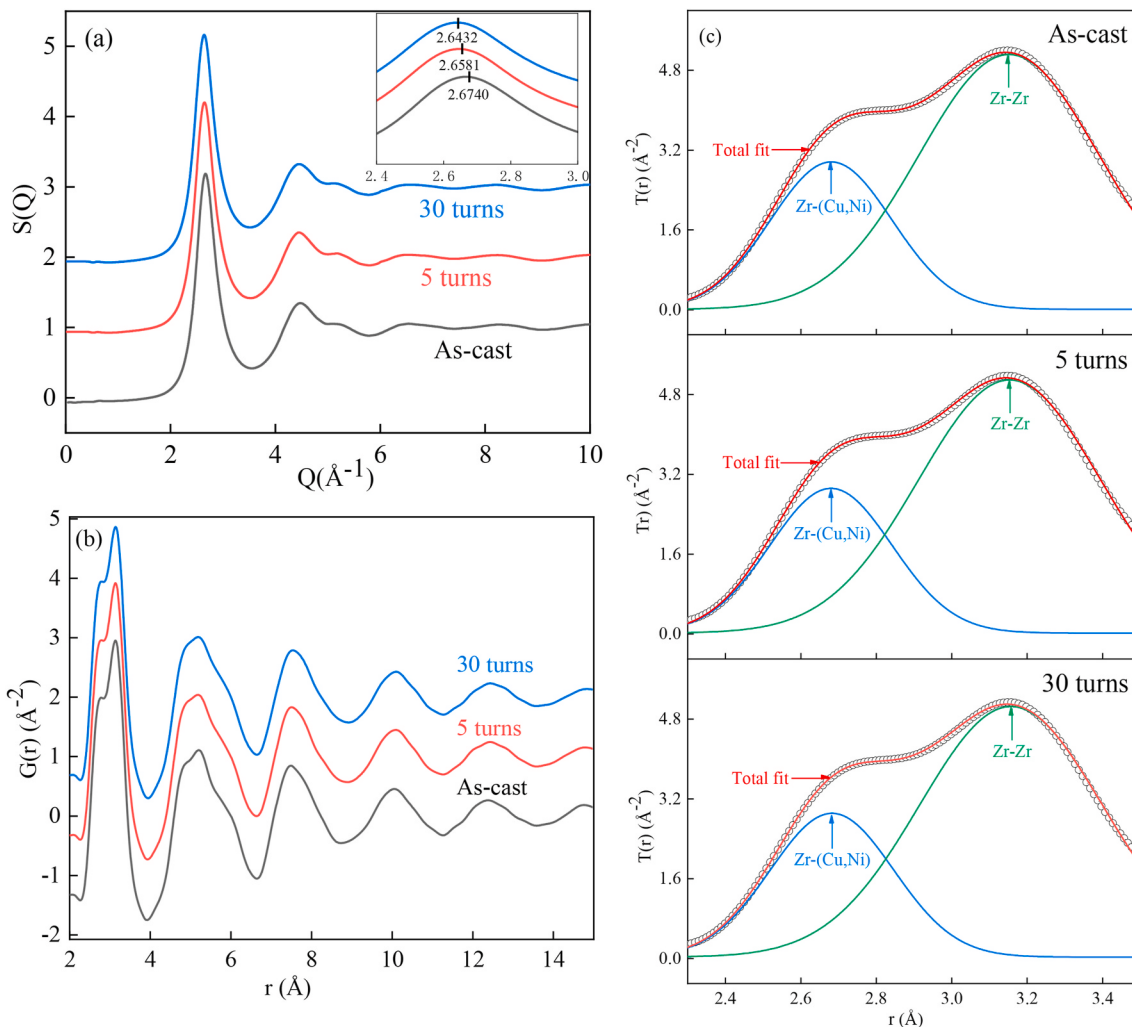


Fig. 3. The structure factor, $S(Q)$, and pair distribution functions derived from synchrotron XRD. (a) The structure factor, (b) the overall tendency of the pair distribution functions, and (c) the best fit of a linear combination of Gaussians to the first-shell peaks of PDFs [$T(r)$].

Table 2
The weight factors of atomic pairs in the Vit105 metallic glass.

i-j	Zr-(Cu, Ni)	Zr-Zr	Zr-(Ti, Al)	Cu-Ni	Ti-Ti	Ti-(Ni, Cu)	Al-(Ni, Cu)
Weight factor	0.365	0.413	0.094	0.081	0.006	0.019	0.023

medium-range ordering up to $\sim 15 \text{ \AA}$, and no significant correlation peaks can be observed after 15 \AA . According to the weight factors (Table 2), the first sub-peak can be assigned mainly to the Zr-(Cu,Ni) pairs, while the Zr-Zr pairs dominate the second sub-peak. Compare to Zr-Zr and Zr-(Cu,Ni), the weights of the other partials are lower. The contribution of these partial with low concentration and weak scattering is ignored in resolving the nearest-neighbor partials. In order to resolve the nearest-neighbor partials from the first PDF peak, the formula $T(r) = 4\pi p_0 r + G(r)$ is used to convert $G(r)$ into $T(r)$, where, p_0 is the mean

density [43]. The atomic pair distribution of amorphous alloys follows the Gaussian distribution, as shown in Fig. 3(c). The corresponding structural parameters of as-cast and HPT specimen are shown in Table 3. The results show that the first peak of all samples split into two sub-peaks located at ~ 2.68 and 3.15 \AA , respectively. The Zr-Zr bond of HPT specimen tends to shift to the right, especially the 30 turns HPT specimen. This suggests that the atomic packing in the nearest neighbors is looser in HPT specimens compared to the as-cast. According to the previous conclusion of S(Q) peak, in the nearest coordination shell, the overall free volume (V_f) of real space increases with HPT.

Fig. 4 shows the TEM and HRTEM observation of the as-cast and HPT-processed BMG specimen. No crystallite precipitations are observed in the as-cast (Fig. 4 (a and d)), and 5 turns HPT specimen (Fig. 4 (b)). Whereas, a large number of nanocrystal precipitates after 30 turns HPT were observed under TEM (Fig. 4 (c)). This is confirmed by HRTEM observation as show in Fig. 4 (e and f), especially the crystalline lattice fringe feature of the precipitates at high resolution in Fig. 4(e and f). These nanocrystals were found to be Cu enriched by EDS (Fig. 5).

Fig. 6 gives the size distribution of nanocrystals precipitates measured and calculated using software ImageJ from TEM images. The average size of the nanocrystals is 45.2 nm. The volume fraction of nanocrystals precipitate after 30 turns HPT is calculated using the relation [44]:

$$f = \left(\frac{-2\pi\bar{d}}{\pi\bar{d} + 8t} \right) \ln(1 - A) \quad (1)$$

where \bar{d} (the average size of nanocrystals) is computed from $\bar{d} = (\sum_{i=1}^n d_i)/m$.

Here m is the number of nanocrystals. The area fraction of nanocrystal precipitates after HPT 30 turns A is 4.9%. The thickness of the foil “ t ” is estimated to be equal to \bar{d} [23]. The volume fraction of nanocrystals precipitates after 30 turns HPT is about 2.83%. To have an accurate statistical result, at least 130 nanocrystals were measured.

4. Discussions

4.1. The effect of free volume on ductility

In this work, the 5 turns HPT specimen shows increased ductility with a slight fall of yield strength exhibiting stable fracture strength in comparison to the as-cast specimen. The increased free volume achieved after 5 turns HPT might be responsible for additional plasticity. Many investigations have also reported the improvement in plasticity with increasing the free volume [45–48]. The plastic flow of BMGs is related to the flow units, which are easily activated in some local atomic locations with high free volume density [49–51]. The loss of free volume increases the viscosity of the BMGs, which leads to a decrease in atomic mobility [52]. Therefore, the stress relaxation during plastic flow becomes more difficult, which will reduce the ductility of BMGs. On the contrary, the large free volume in BMGs facilitates the flow of atoms during straining, which leads to profuse shear bands imparting ductility in BMGs [53]. In this work, synchrotron X-ray results reveals the increase in the free volume of the 5 turns HPT specimen, which may provide additional nucleation sites for shear bands formation. The propagation of large number of shear bands facilitates homogeneous strain distribution during deformation. At the same time, these shear

bands will propagate simultaneously forming secondary and tertiary (sub branches) shear bands, dispersing the applied strain and therefore enhance the ductility of BMGs [54]. As is known, the plastic yielding in BMGs is a result of shear bands [55,56], which are formed by torrential wave of shear transformation zones (STZs). The yield (and flow) stress is always the critical stress required to propagate the initial shear band or to maintain the slip of the existing shear bands [57]. Hence, the yield process of amorphous alloy is closely related to the initiation and propagation of shear bands. The increased free volume in the HPT process make shear bands easy to initiate and propagate. This means that shear bands can initiate and propagate at low flow stress. This explains the difference in yield stress after 5 turns HPT compared to the as-cast specimen.

4.2. Strengthening from nanocrystal precipitates

As shown in Table 4, compared to the as-cast specimen, the change in yield stress of 5 turns and 30 turns HPT specimen is -110 MPa and 139 MPa, respectively. The reduced yield stress of the 5 turns HPT specimen is reasonably due to the softening caused by the increase in free volume. With this same trend, the additional increase of free volume of the 30 turns HPT specimen would lead to further decrease in yield stress than that of the 5 turns HPT specimen. However, the yield stress of the 30 turns HPT specimen did not decrease but increased by 139 MPa instead. This indicates that there must be other strengthening effect, which is strong enough to prevail over the decreasing effect on strength from free volume. The nano-crystalline precipitation observed in the 30 turns HPT specimen could be considered to provide such a strengthening effect. Comparing the yield stress change of the 5 turns and 30 turns HPT specimen, and their free volume data given in Table 4, the strengthening effect of such precipitation hardening in the 30 turns HPT specimen could amount to > 249 MPa.

Due to the small size of the nano-crystalline precipitates inside the amorphous matrix, there is almost no contribution of dislocations during the plastic deformation of amorphous-crystalline composites. Therefore, the strength enhancement induced by dislocation motion is not sensible [53]. In this case, the phase mixture model is considered suitable to estimate the strength of amorphous-crystalline composites [53,58,59]. The strength of the amorphous-crystalline is composed of the strength of the nanocrystals and the amorphous matrix, the strengthening due to the HPT deformation-induced nanocrystals, $\Delta\sigma$, is estimated as [53]:

$$\Delta\sigma = \Delta f_{am}\sigma_{am} + \Delta f_c\sigma_c \quad (2)$$

The nominal strength of the nanocrystals is expected to be 10–12 GPa [53]. $\Delta f_{am}\sigma_{am}$ and $\Delta f_c\sigma_c$ of the amorphous-crystalline composite obtained by 30 turns HPT processing, is thus estimated to be -47 MPa and 283–340 MPa, respectively. And σ_c , the precipitation hardening effect estimated by the phase mixture model (2) is thus 236–293 MPa. This estimation is in good agreement with the experimental observation that the precipitation hardening effect is > 249 MPa. These strength estimations and comparison are summarized in Table 4, together with the strain hardening effect. It is also shown in the table that strain hardening observed in the experimental specimen increase monotonically with free volume.

4.3. Synergistic effect of free volume and nanocrystals on ductility

In the present work, the mechanical properties of the amorphous-crystalline composites processed by 30-turn HPT show significant improvement in the strength and ductility simultaneously. This agrees with some of previous investigations [13,14]. However, some other investigations showed loss of ductility in the amorphous-crystalline composites [18,19] compared to their monolithic amorphous counterparts. This provides a real challenge to identify the controlling parameters and quantitatively predict the ductility behavior in the parameter space. To deal with such a challenge, the ductilization effect from the

Table 3

Structural parameters of the as-cast and HPT specimen.

	$Q_1 (\text{\AA}^{-1})$	$V_a (\text{\AA}^3)$	$V_f (\text{\AA}^3)$	Peak position(\text{\AA})	
				Zr-(Cu,Ni)	Zr-Zr
As-cast	2.6740	18.06	0.9030	2.6821	3.1545
5 turns	2.6581	18.31	0.9155	2.6814	3.1559
30 turns	2.6432	18.55	0.9275	2.6841	3.1597

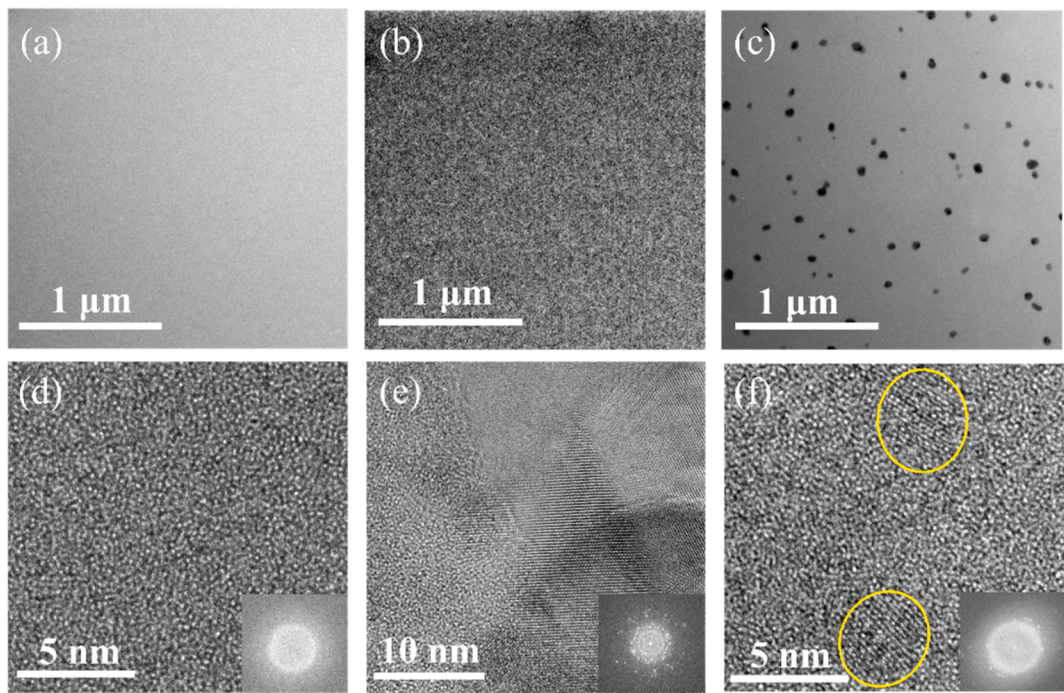


Fig. 4. The TEM micrographs of (a) as-cast, (b) 5 turns HPT and (c) 30 turns HPT specimen. The HRTEM micrographs of (d) as-cast, (e and f) after 30 turns HPT specimen showing different size nanocrystals; Corresponding inset showing Fast-Fourier-Transformation (FFT) of the HRTEM micrographs.

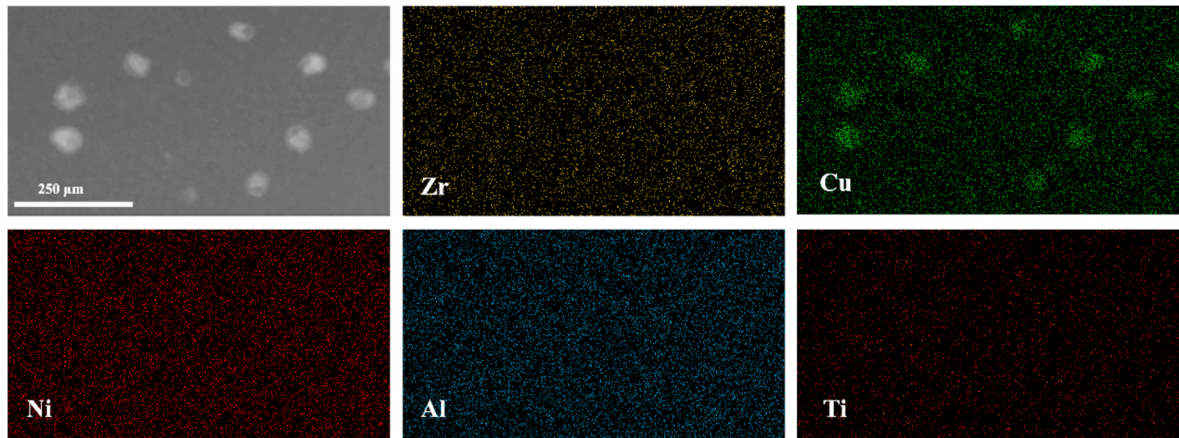


Fig. 5. EDS of the 30 turns HPT BMGs.

increasing free volume as discussed in section 4.1, and the deflection of shear band around crystalline inclusions, could be formulated versus the embrittlement effect caused by the stress concentration at around these crystalline inclusions. The deflection of shear band and embrittlement effect caused by the inter-crystallite spacing is illustrated in Fig. 7.

In general, there is a definite zone around the crystalline inclusion (Fig. 7(I)) that can attract the deflection of the shear bands, thus affecting the propagation of the shear bands and improving the ductility of the amorphous-crystalline composites, as shown in Fig. 7(II), [23,24]. For the manifestation of this beneficial effect, there should be enough crystallites to deflect shear bands. It is clear that the probability P for the manifestation of this deflection would be proportional to the inverse of the inter-crystallite spacing L and the density of the shear bands ω :

$$P = D\omega/L \quad (3)$$

where D is the coefficient of the proportion with a dimension of area. Combined with the general values of shear bands density and inter-

crystallite spacing, D is not larger than 10^4 nm^2 when the range of P is 0–1.

$P = 1$ means that the shear bands are assured to interact with the affected zones around the crystalline inclusion, that is, the shear bands are assured to deflect. Therefore, the relationship between top limit of inter-crystallite spacing L_T and shear bands density ω would be:

$$L_T = D\omega \quad (4)$$

The shear bands density is proportional to the nucleation rate of the shear bands. In steady-state flow, under shear load, the activation rate \dot{s} of STZ follows the equation [52]:

$$\dot{s} = v_0 \cdot \exp\left(-\frac{q - \tau V}{k_B T}\right) \quad (5)$$

where τ is the applied shear stress, and k_B the Boltzmann constant, T the absolute temperature, and v_0 the attempt frequency, is of the order of the Debye frequency for a sufficiently local process. The Debye frequency of

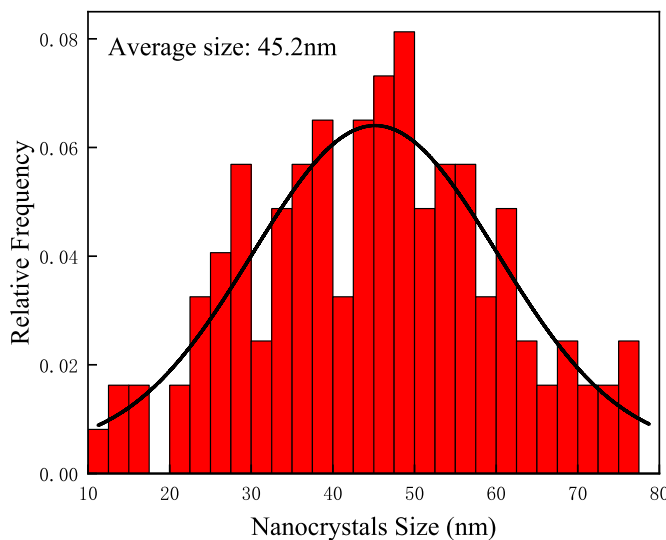


Fig. 6. The size distribution of nanocrystal precipitated from 30 turns HPT specimen.

zirconium is about 6.37×10^{13} rad/s, of copper is about 7.98×10^{13} rad/s, of aluminum is about 9.66×10^{13} rad/s, of nickel is about 9.88×10^{13} rad/s, and of titanium is about 9.13×10^{13} rad/s [60–62]. In terms of weighted average by atomic percentage, the Debye frequency of Vit105 is about 7.64×10^{13} rad/s. V is the activation volume which is the product of the characteristic STZs volume V_{STZ} and shear strain γ of about 0.1 [63]. The volume of STZ is about 10–100 atoms in Zr-based BMGs [64], so it can be expressed as NV_a (the product of total atoms in STZ and the average atomic volume), or $NV_f/(1-n)$. The characteristic activation energy for an STZ operation q can be thought of as a quantity related to Poisson's ratio, temperature dependent shear modulus and so on, and the value is approximately 0.32ev [65]. Therefore, the top limit of crystallites spacing assuring deflection of shear bands is positively correlated to the shear bands nucleation rate and can be expressed as:

$$\omega = c s \quad (6)$$

Table 4
Mechanical properties of the as-cast and HPT specimen.

	ΔYS (MPa)	Strain hardening (MPa)	Precipitation hardening (exp) (MPa)	V_f (\AA^3)	f_c (%)	Precipitation hardening (cal) (MPa)
As-cast	-	69	-	0.9030	-	-
5 turns	-110	194	-	0.9155	-	-
30 turns	+139	230	>249	0.9275	2.83	236–293

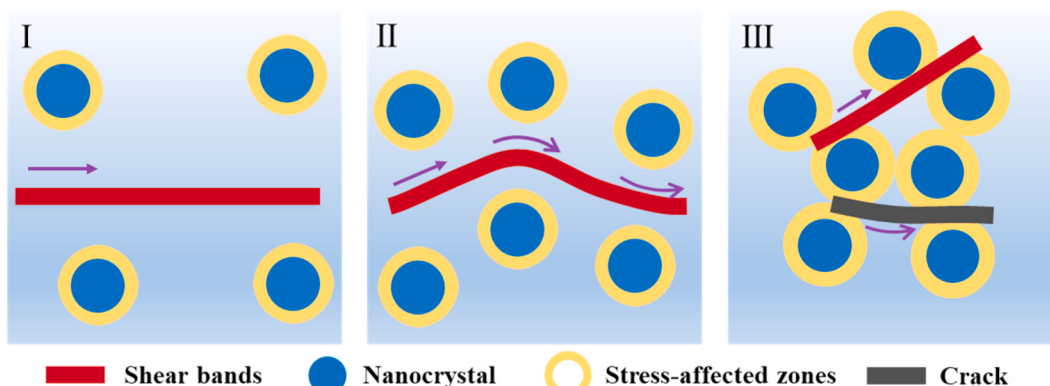


Fig. 7. Schematic diagram explaining the effect of inter-crystallite spacing on deflection of shear bands and embrittlement.

with c as a coefficient of the proportion. Substituting equations (5) and (6) into (4) would lead to the following relationship between top limit of inter-crystallite spacing and the free atomic volume V_f as:

$$L_T = Dcv_0 \cdot \exp\left(-\frac{q - \tau\gamma NV_f / (1-n)}{k_B T}\right) \quad (7)$$

L_T given by equation (7) presents a top limit boundary, in the two dimensional space coordinated by free volume (V_f) and inter-crystallite spacing (L), for the ductilization-embrittlement transition by the inclusion of crystallites in the crystalline-amorphous composite, delineated by the capability of the crystallites to deflect shear bands in the amorphous matrix.

On the other side, stress-affected zones (SAZ) form around the crystallites in certain range. If the inter-crystallites spacing L is too small that the SAZ from neighboring crystallites overlaps, significant stress concentration develops that might lead to crack initiation (Fig. 7(III)) [40], and this yields a bottom limit of the inter-crystallites spacing L_B for the ductile-brittle transition of the crystalline-amorphous composite. In an elastic matrix, the stress σ_{ij} , induced by a crystallite inclusion decays with the distance R from the inclusion, and can be expressed by equation [66]:

$$\sigma_{ij}(x) = \frac{\mu(1+\nu)}{6\pi(1-\nu)} \Delta V \left(\frac{\delta_{ij}}{R^3} - \frac{3x_i x_j}{R^5} \right) \quad (8)$$

where, ΔV is the volume change caused by the crystallites, which is of about 5% of the original amorphous volume in the present system [67]. μ is the shear modulus and ν is the Poisson's ratio of the elastic body, taken here in the present case from the amorphous matrix. $R = |x|$ and x_i and x_j are the i-th and j-th component of coordinate vector x , respectively. δ_{ij} is the Kronecker delta. Assume σ_C is the critical stress required for crack initiation, the maximum distance R_M from the crystallite inclusion that assures crack initiation is related to the matrix shear modulus μ by:

$$R_M^3 = \frac{\mu(1+\nu)}{6\pi(1-\nu)} \frac{\Delta V \cdot a}{\sigma_C} \quad (9)$$

where a is a constant. The relationship between the shear modulus μ of the matrix amorphous alloy and the free volume V_f is given by Ref. [68]:

$$\mu = C \frac{k_B T}{r^2 [V_f/(1-n)]^{1/3}} \quad (10)$$

where, C is a constant of 0.0276 [68]. r^2 is a vibrational parameter associated with the structure, and based on the size of the atomic volume, the value is about 0.03 \AA^2 when the atomic volume is close to 20 \AA^3 [68]. Therefore, bottom limit of inter-crystallite spacing that assures crack initiation in the SAZ and the average atomic volume is as follows:

$$L_B = 2R_M = \left[\frac{8Ck_B T(1+\nu)\Delta V \cdot a}{r^2 \sigma_c \cdot 6\pi(1-\nu)} \right]^{1/3} [V_f/(1-n)]^{-1/9} \quad (11)$$

Substituting all the parameter values into Eqs. (7) and (11) yields the following equations for the top and bottom limit of inter-crystallite spacing as functions of free volume as:

$$L_T \approx 64.3 \cdot \exp(0.868V_f) \quad (12-1)$$

$$L_B \approx 42.2 \cdot V_F^{-1/9} \quad (12-2)$$

The top and bottom limit of inter-crystallite spacing, L_T and L_B , which assure shear band deflection and crack initiation respectively by the effect the crystallite inclusions, delineates a window in the space of free volume and inter-crystallite spacing. Where the ductility of the composite is enhanced by the composition of the crystallite inclusions, as shown in Fig. 8. Outside the window, compositing of the crystallite inclusions in the amorphous matrix might lead to embrittlement.

Once the nanocrystals volume fraction and the average size are known, the average inter-crystallite spacing can be estimated by Ref. [26]:

$$L = \bar{d} \sqrt[3]{\frac{\pi}{6f}} \quad (13)$$

where \bar{d} and f are the average nanocrystals diameter and volume fraction. In this way, the average spacing between the nanocrystals of 30 turns HPT specimen is estimated to 117.8 nm and the free volume of the sample of 30 turns HPT specimen is 0.9275 \AA^3 from Table 3. This identifies a data point within the above mentioned window, as shown by the orange star in Fig. 8, thus ductility is enhanced by the inclusion of the nano-crystallites. Similar data of free volume and inter-crystallite spacing are taken from literature [19,69], and they give additional example of data point within the window, as well as outside the window, as shown by the blue square and purple hexagonal. They all fits well

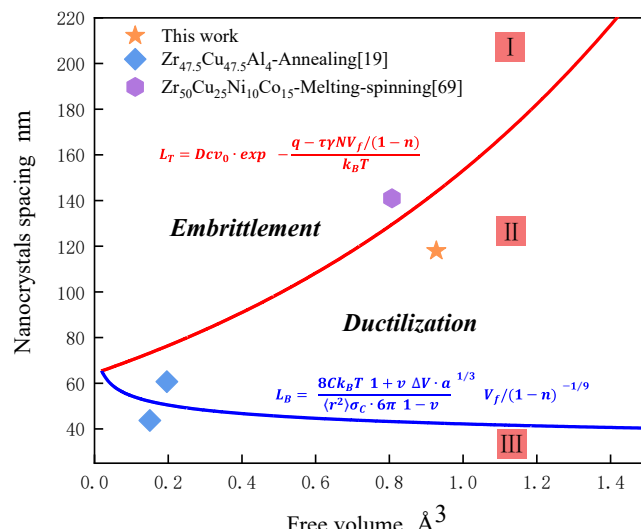


Fig. 8. The ductilitization window in the space of free volume v.s. inter-crystallite spacing.

with prediction of the ductilitization window delineated by the present model.

Fig. 8 shows the relationship established between bottom limit (L_B) and top limit (L_T) of the crystallite spacing w.r.t the free volume inside the amorphous crystalline composite. The left of the intersection between red and blue line suggests that when the free volume of the amorphous matrix is too low, the stress concentration near the crystalline precipitate will overcome the stress required to deflect the shear bands, thereby generating crack. Consequently, the amorphous crystalline composite would be brittle. This notion can be confirmed by the fact that when producing crystallites by annealing the amorphous alloy, this frequently leads to reduction of ductility, or embrittlement of the composite [18,19]. Additionally, as the free volume in the matrix increase, a window between the partition of L_T and L_B (Fig. 8) takes shape. If the spacing between crystallites and free volume of amorphous crystalline composite is within that window, the composite would be ductile. Hence, to ensure plasticity in an amorphous-crystalline composite, both the free volume in the amorphous matrix and inter-crystallite spacing should be considered.

The microscopic processes of initiation, propagation, and obstruction of the shear bands are closely related to macroscopic behavior of yield, fracture and plastic deformation of BMGs [70]. The change of free volume and nanocrystal dispersions has significant influence on shear bands [25], and thus determines macroscopic behavior of the material. For amorphous-crystalline composites, in addition to the increase in ductility due to the increase in the free volume inside the amorphous matrix, the ductility may also be affected by the structural changes caused by the precipitation of nanocrystals. Due to the increase of free volume, the shear bands will grow extensively towards the nanocrystals, subsequently changing the propagation direction [24]. This leads to further stress depletion and hence delaying fracture. Simultaneously, nanocrystals will also block the motion of shear bands, inhibiting the formation of cracks [71]. Therefore, the synergistic effect of free volume and dispersion of nanocrystals precipitations are accountable for plasticity of the amorphous-crystalline composites, which is manifested in the present work by 30-turn HPT processed Vit105 alloy. This study provides a good example and physical understanding on increasing strength as well as ductility of BMGs simultaneously by dispersion of crystallite inclusions and free volume in amorphous-crystalline composites.

5. Conclusion

BMG $\text{Zr}_{52.5}\text{Cu}_{17.9}\text{Al}_{10}\text{Ni}_{14.6}\text{Ti}_5$ (Vit105) is processed by High Pressure Torsion up to 30 turns at room temperature, the structure evolution and mechanical property are characterized by HRTEM, Synchrotron X-ray diffraction and tensile testing. The synergistic enhancement of strength and ductility of the alloy through the increase of free volume and nanocrystal precipitates are modeled. The following conclusions can be drawn from the present research:

- 1) Free volume in the BMGs is increased by the high-pressure torsion, from $\sim 0.9030 \text{ \AA}^3$ in the as-cast specimen to $\sim 0.9155 \text{ \AA}^3$ in the 5 turns HPT specimen and $\sim 0.9275 \text{ \AA}^3$ in the 30 turn HPT specimen; atomic pair distribution analysis suggests that the atomic packing in the nearest neighbors is looser in HPT specimens compared to the as-cast one, and this increases the free volume in HPT specimens.
- 2) Precipitation of Cu-rich nanocrystal is observed in the 30 turns HPT specimen, with an average diameter of 45 nm , and a volume fraction of 2.83% . The precipitation hardening leads to increase in the yield stress and ultimate strength of the BMG, and this strengthening follows the rule of phase mixture model.
- 3) The simultaneous increase in both strength and elongation is achieved by 30 turns HPT processing of as-cast Vit105 alloy. The yield stress, ultimate tensile strength and elongation of the alloy are increased from 1654 MPa , 1723 MPa and 0.06% in the as-cast

- specimen to 1793 MPa, 2023 MPa and 0.45% in the 30 turns HPT specimen, respectively. Significant improvement in elongation and strain hardening is obtained with the increase of free volume by HPT processing.
- 4) The synergistic effect of free volume and nanocrystal precipitation on the ductility of amorphous-crystallite composite is quantitatively approached through modelling. By implementing the model, a relationship between bottom limit and top limit of the crystallite spacing w.r.t the free volume is established. This elucidates the necessary conditions required for ductilization in amorphous-crystalline composites.

CRediT authorship contribution statement

Zhi Qiang Ren: Writing - original draft, Methodology, Data curation, Writing - review & editing. **A.A. Churakova:** Resources. **Xiang Wang:** Investigation, Data curation. **Sunkulp Goel:** Writing - review & editing. **Si Nan Liu:** Data curation. **Ze Sheng You:** Resources. **Ying Liu:** Investigation. **Si Lan:** Resources. **D.V. Gunderov:** Resources. **Jing Tao Wang:** Conceptualization, Methodology, Writing - review & editing, Funding acquisition. **R.Z. Valiev:** Resources, Funding acquisition.

Declaration of competing interest

The authors declare that they have no known competing financial interests or personal relationships that could have appeared to influence the work reported in this paper.

Acknowledgements

This work was supported by the Natural Science Foundation of China (Grant No. 51520105001, 51871120). RVZ acknowledge the research grant SPbSU in the framework of Call 3 project (id 26130576) and in part support from the Ministry of Education of the Russian Federation under grant agreement No. 0838-2020-0006. Prof. Ren YANG is greatly acknowledged for his help in conducting the Synchrotron X-ray diffraction experiment. This research used the resources of the Advanced Photon Source, a US Department of Energy (DOE) Office of Science User Facility operated for the DOE Office of Science by Argonne National Laboratory under Contract no. DE-AC02-06CH11357.

References

- [1] A. Inoue, W. Zhang, T. Zhang, K. Kurosaka, High-strength Cu-based Bulk glassy alloys in Cu-Zr-Ti and Cu-Hf-Ti ternary systems, *Acta Mater.* 49 (2001) 2645–2652.
- [2] A.I. Salimon, M.F. Ashby, Y. Bréchet, A.L. Greer, Bulk metallic glasses: what are they good for? *Mater. Sci. Eng., A* 375–377 (2004) 385–388.
- [3] R.D. Conner, W.L. Johnson, N.E. Paton, W.D. Nix, Shear bands and cracking of metallic glass plates in bending, *J. Appl. Phys.* 94 (2003) 904–911.
- [4] Y.K. Xu, H. Ma, J. Xu, E. Ma, Mg-based bulk metallic glass composites with plasticity and gigapascal strength, *Acta Mater.* 53 (2005) 1857–1866.
- [5] Z.F. Zhang, H. Zhang, B.L. Shen, A. Inoue, J. Eckert, Shear fracture and fragmentation mechanisms of bulk metallic glasses, *Phil. Mag. Lett.* 86 (2006) 643–650.
- [6] J. Shen, W.Z. Liang, J.F. Sun, Formation of nanowaves in compressive fracture of a less-brittle bulk metallic glass, *Appl. Phys. Lett.* 89 (2006) 121908.
- [7] M. Chen, A. Inoue, W. Zhang, T. Sakurai, Extraordinary plasticity of ductile bulk metallic glasses, *Phys. Rev. Lett.* 96 (2006) 245502.
- [8] R.J. Hebert, J.H. Pérezko, H. Rösner, G. Wilde, Dislocation formation during deformation-induced synthesis of nanocrystals in amorphous and partially crystalline amorphous Al88Y7Fe5 alloy, *Scripta Mater.* 54 (2006) 25–29.
- [9] Y.H. Liu, G. Wang, R.J. Wang, D.Q. Zhao, M.X. Pan, W.H. Wang, Super plastic bulk metallic glasses at room temperature, *Science* 315 (2007) 1385–1388.
- [10] H. Choi-Yim, W.L. Johnson, Bulk metallic glass matrix composites, *Appl. Phys. Lett.* 71 (1997) 3808–3810.
- [11] R.T. Qu, Q.S. Zhang, Z.F. Zhang, Achieving macroscopic tensile plasticity of monolithic bulk metallic glass by surface treatment, *Scripta Mater.* 68 (2013) 845–848.
- [12] R.T. Qu, M. Calin, J. Eckert, Z.F. Zhang, Metallic glasses: notch-insensitive materials, *Scripta Mater.* 66 (2012) 733–736.
- [13] C.C. Hays, C.P. Kim, W.L. Johnson, Microstructure controlled shear band pattern formation and enhanced plasticity of bulk metallic glasses containing in situ formed ductile phase dendrite dispersions, *Phys. Rev. Lett.* 84 (2000) 2901–2904.
- [14] U. Kühn, J. Eckert, N. Mattern, L. Schultz, ZrNbCuNiAl bulk metallic glass matrix composites containing dendritic bcc phase precipitates, *Appl. Phys. Lett.* 80 (2002) 2478–2480.
- [15] A. Inoue, C. Fan, J. Saida, T. Zhang, High-strength Zr-based bulk amorphous alloys containing nanocrystalline and nanoquasicrystalline particles, *Sci. Technol. Adv. Mater.* 1 (2000) 73–86.
- [16] J. Eckert, A. Reger-Leonhard, B. Weiß, M. Heilmair, Nanostructured materials in multicomponent alloy systems, *Mater. Sci. Eng.* 301 (2001) 1–11.
- [17] C. Fan, A. Inoue, Ductility of bulk nanocrystalline composites and metallic glasses at room temperature, *Appl. Phys. Lett.* 77 (2000) 46–48.
- [18] A. Concstell, G. Alcalá, S. Mató, T.G. Woodcock, A. Gebert, J. Eckert, M.D. Baró, Effect of relaxation and primary nanocrystallization on the mechanical properties of Cu60Zr22Ti18 bulk metallic glass, *Intermetallics* 13 (2005) 1214–1219.
- [19] R. Wei, X.L. Wang, S. Yang, F. Jiang, L. He, Formation of CuZr-based bulk metallic glass composites containing nanometer-scale B2-CuZr phase through sub-Tg annealing, *J. Alloys Compd.* 617 (2014) 699–706.
- [20] M.E. Launey, R. Busch, J.J. Krutzic, Effects of free volume changes and residual stresses on the fatigue and fracture behavior of a Zr-Ti-Ni-Cu-Be bulk metallic glass, *Acta Mater.* 56 (2008) 500–510.
- [21] M.L. Lind, G. Duan, W.L. Johnson, Isoconfigurational elastic constants and liquid fragility of a bulk metallic glass forming alloy, *Phys. Rev. Lett.* 97 (2006), 015501.
- [22] R. Bhowmick, R. Raghavan, K. Chattopadhyay, U. Ramamurty, Plastic flow softening in a bulk metallic glass, *Acta Mater.* 54 (2006) 4221–4228.
- [23] B.A. Sun, K.K. Song, S. Pauly, P. Gargarella, J. Yi, G. Wang, C.T. Liu, J. Eckert, Y. Yang, Transformation-mediated plasticity in CuZr based metallic glass composites: a quantitative mechanistic understanding, *Int. J. Plast.* 85 (2016) 34–51.
- [24] S. Pauly, G. Liu, S. Gorantla, G. Wang, U. Kühn, D.H. Kim, J. Eckert, Criteria for tensile plasticity in Cu-Zr-Al bulk metallic glasses, *Acta Mater.* 58 (2010) 4883–4890.
- [25] S.H. Joo, D.H. Pi, A.D. Setyawan, H. Kato, M. Janecek, Y.C. Kim, S. Lee, H.S. Kim, Work-hardening induced tensile ductility of bulk metallic glasses via high-pressure torsion, *Sci. Rep.* 5 (2015) 9660.
- [26] S. Hőbör, Á. Révész, P.J. Szabó, A.P. Zhilyaev, V.K. Kis, J.L. Lábár, Z. Kovács, High pressure torsion of amorphous Cu60Zr30Ti10 alloy, *J. Appl. Phys.* 104 (2008), 033525.
- [27] E.V. Boltynjuk, D.V. Gunderov, E.V. Ubyivovk, M.A. Monclús, L.W. Yang, J. Molina-Aldareguia, A.I. Tyurin, A.R. Kilmamatov, A.A. Churakova, A.Y. Churyumov, R.Z. Valiev, Enhanced strain rate sensitivity of Zr-based bulk metallic glasses subjected to high pressure torsion, *J. Alloys Compd.* 747 (2018) 595–602.
- [28] D.V. Gunderov, A.A. Churakova, E.V. Boltynjuk, E.V. Ubyivovk, V.V. Astanin, R.N. Asfandiyarov, R.Z. Valiev, W. Xiaoang, J.T. Wang, Observation of shear bands in the Vitreloy metallic glass subjected to HPT processing, *J. Alloys Compd.* 800 (2019) 58–63.
- [29] H. Wang, Z.S. You, L. Lu, Kinematic and isotropic strain hardening in copper with highly aligned nanoscale twins, *Mater. Res. Lett.* 6 (2018) 333–338.
- [30] R.T. Qu, Z.F. Zhang, A universal fracture criterion for high-strength materials, *Sci. Rep.* 3 (2013) 1117.
- [31] Z.F. Zhang, J. Eckert, L. Schultz, Fatigue and fracture behavior of bulk metallic glass, *Metall. Mater. Trans.* 35 (2004) 3489–3498.
- [32] R.T. Qu, Z.Q. Liu, G. Wang, Z.F. Zhang, Progressive shear band propagation in metallic glasses under compression, *Acta Mater.* 91 (2015) 19–33.
- [33] B.A. Sun, H.B. Yu, W. Jiao, H.Y. Bai, D.Q. Zhao, W.H. Wang, Plasticity of ductile metallic glasses: a self-organized critical state, *Phys. Rev. Lett.* 105 (2010), 035501.
- [34] R.T. Qu, Z.F. Zhang, Compressive fracture morphology and mechanism of metallic glass, *J. Appl. Phys.* 114 (2013) 193504.
- [35] R.T. Qu, M. Stoica, J. Eckert, Z.F. Zhang, Tensile fracture morphologies of bulk metallic glass, *J. Appl. Phys.* 108 (2010), 063509.
- [36] K.K. Song, S. Pauly, Y. Zhang, S. Scudino, P. Gargarella, K.B. Surreddi, U. Kühn, J. Eckert, Significant tensile ductility induced by cold rolling in Cu47.5Zr47.5Al5 bulk metallic glass, *Intermetallics* 19 (2011) 1394–1398.
- [37] S. Scudino, K.B. Surreddi, Shear band morphology and fracture behavior of cold-rolled Zr52.5Ti5Cu18Ni14.5Al10 bulk metallic glass under tensile loading, *J. Alloys Compd.* 708 (2017) 722–727.
- [38] D. Ma, A.D. Stoica, X.L. Wang, Power-law scaling and fractal nature of medium-range order in metallic glasses, *Nat. Mater.* 8 (2009) 30–34.
- [39] D. Turnbull, M.H. Cohen, On the free-volume model of the liquid-glass transition, *J. Chem. Phys.* 52 (1970) 3038–3041.
- [40] Y. Xu, J. Fang, H. Gleiter, H. Hahn, J. Li, Quantitative determination of free volume in Pd40Ni40P20 bulk metallic glass, *Scripta Mater.* 62 (2010) 674–677.
- [41] Y. Xu, Y. Zhang, J. Li, H. Hahn, Enhanced thermal stability and hardness of Zr46Cu39.2Ag7.8Al7 bulk metallic glass with Fe addition, *Mater. Sci. Eng., A* 527 (2010) 1444–1447.
- [42] B. Shi, Y. Xu, C. Li, W. Jia, Z. Li, J. Li, Evolution of free volume and shear band intersections and its effect on hardness of deformed Zr64.13Cu15.75Ni10.12Al10 bulk metallic glass, *J. Alloys Compd.* 669 (2016) 167–176.
- [43] D.A. Dimitrov, H. Röder, A.R. Bishop, Peak positions and shapes in neutron pair correlation functions from powders of highly anisotropic crystals, *Phys. Rev. B* 64 (2001), 014303.
- [44] S. Pauly, S. Gorantla, G. Wang, U. Kühn, J. Eckert, Transformation-mediated ductility in CuZr-based bulk metallic glasses, *Nat. Mater.* 9 (2010) 473–477.
- [45] J. Gu, M. Song, S. Ni, X. Liao, S. Guo, Improving the plasticity of bulk metallic glasses via pre-compression below the yield stress, *Mater. Sci. Eng., A* 602 (2014) 68–76.

- [46] S. Mandal, A.J. Kailath, Enhanced plasticity of Cu-Zr-Ti bulk metallic glass and its correlation with fragility, *Metall. Mater. Trans. 50A* (2018) 199–208.
- [47] F. Farahani, R. Gholamipour, Giant size effect on compressive plasticity of (Zr55Cu30Al10Ni5)99Nb1 bulk metallic glass, *Mater. Sci. Eng., A* 651 (2016) 968–975.
- [48] L.Y. Chen, A.D. Setyawan, H. Kato, A. Inoue, G.Q. Zhang, J. Saida, X.D. Wang, Q. P. Cao, J.Z. Jiang, Free-volume-induced enhancement of plasticity in a monolithic bulk metallic glass at room temperature, *Scripta Mater.* 59 (2008) 75–78.
- [49] A.S. Argon, Plastic deformation in metallic glasses, *Acta Mater.* 27 (1978) 47–58.
- [50] Z. Lu, W. Jiao, W.H. Wang, H.Y. Bai, Flow unit perspective on room temperature homogeneous plastic deformation in metallic glasses, *Phys. Rev. Lett.* 113 (2014), 045501.
- [51] Z. Wang, B.A. Sun, H.Y. Bai, W.H. Wang, Evolution of hidden localized flow during glass-to-liquid transition in metallic glass, *Nat. Commun.* 5 (2014) 5823.
- [52] Christopher A. Schuh, T.C. Hufnagel, U. Ramamury, Mechanical behavior of amorphous alloys, *Acta Mater.* 55 (2007) 4067–4109.
- [53] J.-C. Lee, Y.-C. Kim, J.-P. Ahn, H.-S. Kim, S.-H. Lee, B.-J. Lee, Deformation-induced nanocrystallization and its influence on work hardening in a bulk amorphous matrix composite, *Acta Mater.* 52 (2004) 1525–1533.
- [54] L.Q. Xing, Y. Li, K.T. Ramesh, J. Li, T.C. Hufnagel, Enhanced plastic strain in Zr-based bulk amorphous alloys, *Phys. Rev. B* 64 (2001) 180201.
- [55] W.L. Johnson, K. Samwer, A universal criterion for plastic yielding of metallic glasses with $a(T/T_g)^{2/3}$ Temperature dependence, *Phys. Rev. Lett.* 95 (2005) 195501.
- [56] M.W. Chen, Mechanical behavior of metallic glasses: microscopic understanding of strength and ductility, *Annu. Rev. Mater. Res.* 38 (2008) 445–469.
- [57] J. Das, M.B. Tang, K.B. Kim, R. Theissmann, F. Baier, W.H. Wang, J. Eckert, Work-Hardenable" ductile bulk metallic glass, *Phys. Rev. Lett.* 94 (2005), 205501.
- [58] H.S. Kim, S.I. Hong, A model of the ductile-brittle transition of partially crystallized amorphous Al-Ni-Y alloys, *Acta Mater.* 47 (1999) 2059–2066.
- [59] H.S. Kim, Strengthening mechanisms of Zr-based devitrified amorphous alloy nanocomposites, *Scripta Mater.* 48 (2003) 43–49.
- [60] G. Tetzner, R. Schrader, Über Gitterstörungen, Debye-Temperatur und Grenzfrequenz von mechanisch aktiviertem Aluminiumpulver, *Krist. Tech.* 9 (1974) 697–702.
- [61] J. Prakash, B.S. Semwal, P.K. Sharma, Phonon frequency distribution functions of copper, nickel and vanadium, *Acta Phys. Acad. Sci. Hungar.* 30 (1971) 231–240.
- [62] R.R. Rao, A. Rajput, Lattice specific heat and thermal expansion of titanium, *Phys. Rev. B* 19 (1979) 3323–3328.
- [63] M. Heggen, M. Feuerbacher, Creation and annihilation of free volume during homogeneous flow of a metallic glass, *J. Appl. Phys.* 97 (2005), 033506.
- [64] A. Reger-Leonhard, M. Heilmayer, J. Eckert, Newtonian flow of Zr55Cu30Al10Ni5 bulk metallic glassy alloys, *Scripta Mater.* 43 (2000) 459–464.
- [65] D. Klaumünzer, R. Maaß, J.F. Löfller, Stick-slip dynamics and recent insights into shear banding in metallic glasses, *J. Mater. Res.* 26 (2011) 1453–1463.
- [66] W. Cai, R.B. Sills, D.M. Barnett, W.D. Nix, Modeling a distribution of point defects as misfitting inclusions in stressed solids, *J. Mech. Phys. Solid.* 66 (2014) 154–171.
- [67] L.M. Wang, L.L. Sun, W.H. Wang, R.J. Wang, Z.J. Zhan, D.Y. Dai, W.K. Wang, Elastic constants of Pd39Ni10Cu30P21 bulk metallic glass under high pressure, *Appl. Phys. Lett.* 77 (2000) 3734–3736.
- [68] J. Ding, Y.Q. Cheng, H. Sheng, M. Asta, R.O. Ritchie, E. Ma, Universal structural parameter to quantitatively predict metallic glass properties, *Nat. Commun.* 7 (2016) 13733.
- [69] W.H. Gao, X.Y. Yi, X.L. Meng, G. Song, W. Cai, L.C. Zhao, Stress-induced martensitic transformation of Zr 50 Cu 25 Ni 10 Co 15 nanocrystals embedded in an amorphous matrix, *J. Mater. Sci. Technol.* 33 (2017) 276–280.
- [70] A.L. Greer, Y.Q. Cheng, E. Ma, Shear bands in metallic glasses, *Mater. Sci. Eng. R Rep.* 74 (2013) 71–132.
- [71] T. Brink, M. Peterlechner, H. Rösner, K. Albe, G. Wilde, Influence of crystalline nanoprecipitates on shear-band propagation in Cu-Zr-based metallic glasses, *Phys. Rev. Appl.* 5 (2016), 054005.